Microwave-Induced Oscillations in Magnetocapacitance: Direct Evidence for Nonequilibrium Occupation of Electronic States

S. I. Dorozhkin and A. A. Kapustin
Institute of Solid State Physics RAS, 142432 Chernogolovka, Moscow district, Russia

V. Umansky
Department of Physics, Weizmann Institute of Science, 76100 Rehovot, Israel

K. von Klitzing and J. H. Smet
Max-Planck-Institut für Festkörperforschung, Heisenbergstrasse 1, D-70569 Stuttgart, Germany
(Received 8 May 2016; published 17 October 2016)

In a two-dimensional electron system, microwave radiation may induce giant resistance oscillations. Their origin has been debated controversially and numerous mechanisms based on very different physical phenomena have been invoked. However, none of them have been unambiguously experimentally identified, since they produce similar effects in transport studies. The capacitance of a two-subband system is sensitive to a redistribution of electrons over energy states, since it entails a shift of the electron charge perpendicular to the plane. In such a system, microwave-induced magnetocapacitance oscillations have been observed. They can only be accounted for by an electron distribution function oscillating with energy due to Landau quantization, one of the quantum mechanisms proposed for the resistance oscillations.

DOI: 10.1103/PhysRevLett.117.176801

Recent studies of nonequilibrium phenomena in two-dimensional electron systems (2DES) exposed to microwave (MW) radiation have revealed remarkable transport effects. The most prominent one is the appearance of giant microwave-induced magnetoresistance oscillations (MIRO) [1,2]. In the main minima the resistance may approach zero, and so-called zero resistance states develop [3–5]. MIRO have proved to be a general effect as they by now have been observed in semiconductor heterostructures with degenerate two-dimensional electron (GaAs/AlGaAs [1,2], ZnO/MgZnO [6]) and hole (Si/SiGe [7]) systems as well as in nondegenerate 2D electron gases on liquid helium [8] (for additional references, see Ref. [9]). MIRO are periodic in ω/ω_c, where $\omega/2\pi$ is the MW frequency and $\omega_c = eB/m^*$ is the cyclotron frequency. The proposed explanations of MIRO are based on classical or quantum effects, as reviewed in Ref. [9] (see also a recent classical theory [10]). Despite significant progress and a satisfactory description of much of the phenomenology by some of the proposed mechanisms, the theoretical dispute has not been settled since crucial unresolved issues remain. In particular, the absence of a dependence of MIRO on the MW circular polarization direction [11,12] continues to stimulate new theoretical ideas involving edge [13] and contact [14] phenomena and invigorates the debate [15,16]. Magnetotransport experiments alone are likely insufficient to identify unambiguously all mechanisms active in experiment. Apart from MIRO, oscillations of the same periodicity were also found elsewhere in other electronic transport properties. Under MW radiation, voltages and currents develop even in the absence of external sources. These photogalvanic signals [17–19] can be traced back to MIRO and the MW-induced changes in the dc conductivity [20,21]. Therefore, there is clearly a strong need to look at physical quantities other than the conductivity.

Here, using the magnetocapacitance technique and a suitable sample design, we demonstrate that MW radiation generates a nonequilibrium distribution of electrons among the Landau levels oscillating with energy. Such a nonequilibrium distribution function [22–25] represents one of the most elaborate theoretical pictures to account for MIRO as a bulk quantum phenomenon. While capacitive measurements in the presence of the MW radiation have been reported for quasi-2D electrons above a He surface [26,27], in degenerate 2DES the capacitance has not been addressed yet in this microwave context. It has also been widely used for studying the equilibrium 2DES compressibility [28]. The sample consists of a field effect transistor with a back gate and an electron channel that resides in an asymmetric, wide GaAs quantum well (QW) with two occupied subbands. A microwave-induced redistribution of the electrons along the energy scale modifies the occupation of both subbands and is accompanied by a shift of the electrons perpendicular to the QW plane. This shift alters the capacitance which is primarily sensitive to the occupation of the highest subband whose wave function is located closer to the gate. Hence, the capacitance can capture directly microwave-induced oscillations in the electron energy distribution. The sensitivity to vertical electron shifts is what distinguishes this capacitance measurement from all previous transport experiments. A second frequently invoked mechanism [29–34] to explain MIRO involves a microwave-induced impurity scattering assisted displacement of the electrons in the plane. The equations describing MIRO within this displacement model are, except for a temperature-dependent prefactor, identical to the equations obtained from a picture based on a nonequilibrium energy distribution function [24,34]. An unambiguous separation of these two possible contributions is, therefore, nontrivial. The capacitance measurements can not exclude that the displacement mechanism is active in MIRO, as they are not sensitive to lateral displacements. However, they can, without any ambiguity, prove the formation of a nontrivial electron energy distribution function by the microwaves and thereby provide support for a bulk quantum origin of MIRO. We note that a bulk origin of MIRO is also supported either directly or indirectly in Refs. [12,35–37].

We measured two identical Hall bar samples processed side by side on the same piece of a GaAs/AlGaAs heterostructure. The electron system resides in a 60 nm wide GaAs QW. An *in situ* grown back gate allows us to tune the density and measure the capacitance. In these samples the second subband gets populated at total electron density $n_s \approx 1.8 \times 10^{11}$ cm^{-2} for a gate voltage $V_g > 0.15$ V, as will be shown below. Further experimental details are found in the Supplemental Material [38]. The samples were placed in a stainless steel tube with a diameter of 18 mm. It served as an oversized waveguide for the MW radiation whose frequency was varied from 54 to 78 GHz. The measurements were performed in a pumped liquid ^{3}He at 0.5 K.

Figure 1 illustrates the behavior of the longitudinal resistivity, ρ_{xx} [Figs. 1(b) and 1(c)], and variation of the capacitance ΔC [Figs. 1(a) and 1(d)], in the absence and presence of MW radiation for two gate voltages: $V_g = 0$ and 1 V. As shown below, these voltages correspond to one and two occupied subbands, respectively. While the ρ_{xx} curves [Figs. 1(b) and 1(c)] look very similar in both regimes, the magnetocapacitance traces in Figs. 1(a) and 1(d) are qualitatively different. A close inspection allows us to identify four types of $1/B$-periodic oscillations. At high B fields, all ρ_{xx} traces exhibit the well-known Shubnikov–de Haas (SdH) oscillations. The microwaves induce additional, large oscillations in the magnetoresistivity. These are just MIRO. The oscillations in the magnetocapacitance measured in the absence of radiation reflect the oscillations in the thermodynamic density of states (DOS), $\partial n_s/\partial \mu$ [28], brought about by Landau quantization. Here, μ is the chemical potential of the 2DES. The MW radiation suppresses the amplitude of these DOS oscillations in the magnetocapacitance. In the density regime with only one occupied subband (regime I) shown in Fig. 1(d), the suppression is the only effect of the radiation on the capacitance. In contrast, when two subbands are occupied (regime II), the MW radiation induces additional oscillations with a new period. These microwave-induced capacitance oscillations, hereafter referred to as MICO, have been demarcated in Fig. 1(a). They exhibit a node at the same B field where the MIRO have their rightmost zero, i.e., when $\omega = \omega_c$. This is highlighted by the dashed line in Fig. 1. It corresponds to the cyclotron resonance (CR) of electrons with effective mass $m^* = 0.061 m_e$. This value of m^* is close to the $0.059 m_e$ recently obtained [39] from the MIRO periodicity. The observation of MICO is the key experimental result of this Letter.

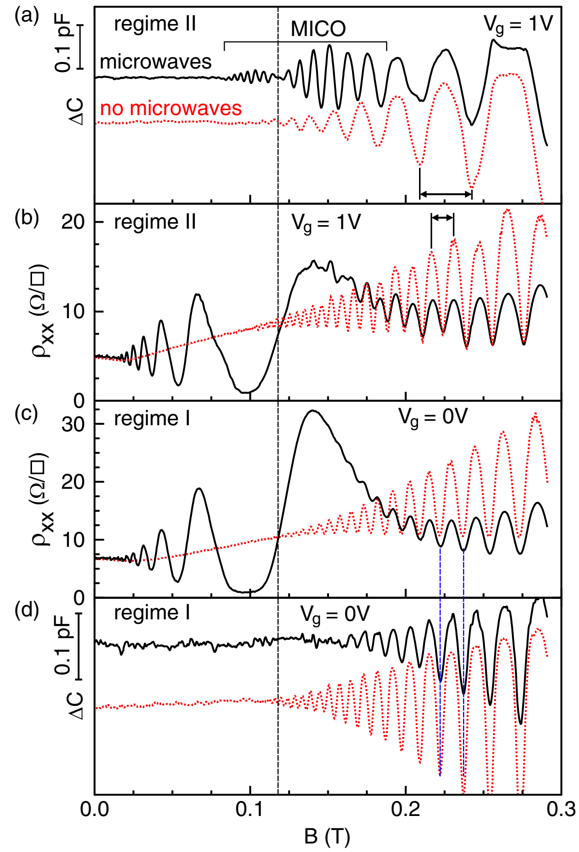

FIG. 1. Magnetocapacitance variation ΔC [(a),(d)] and magnetoresistivity ρ_{xx} [(b),(c)] under MW radiation (solid lines) and without radiation (dashed lines). For the sake of clarity, the dashed magnetocapacitance curves are shifted down by 0.1 pF relative to the solid ones. The data for the two occupied subbands (regime II) are shown in (a) and (b) and for one occupied subband (regime I) in (c) and (d). MW frequency $\omega/2\pi = 54$ GHz. The short vertical lines in (c) and (d) are drawn through the oscillation minima in ρ_{xx} and ΔC.

In Fig. 2(a), MICO have been plotted as a function of $1/B$ for three different MW frequencies to highlight the following: (i) the oscillations are indeed periodic in $1/B$ and the period $1/B_0$ does not depend on the frequency; (ii) the oscillation amplitude indeed reveals a beating pattern with the leftmost node located at the CR (for $m^* = 0.061 m_e$); (iii) when crossing a node the phase of the oscillations jumps by π. This can be seen most easily with the help of the top axis. The abscissa is obtained by

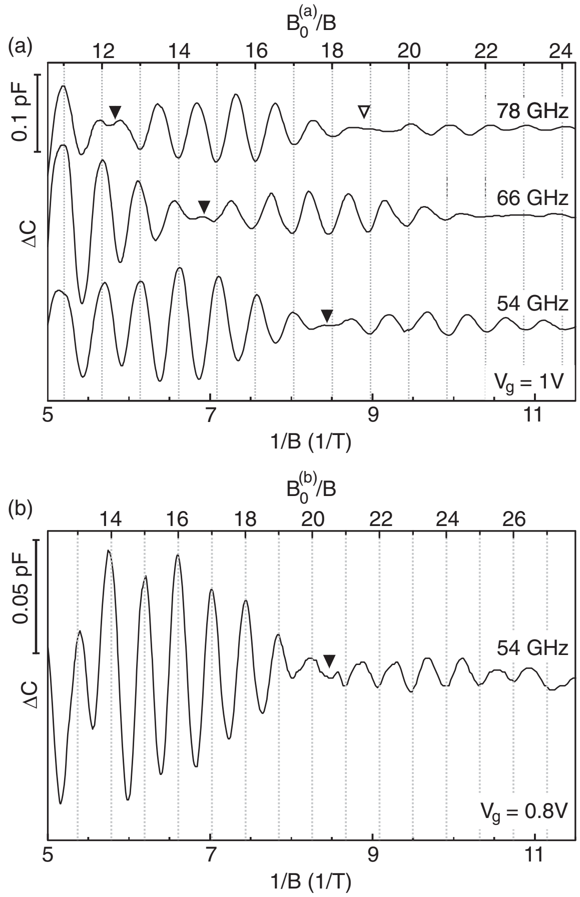

FIG. 2. MICO as a function of inverse magnetic field for different MW frequencies (a) and gate voltages [(a),(b)] shown at the curves. The solid (open) arrows mark the points where $\omega/\omega_c = 1\ (3/2)$ calculated for $m^* = 0.061 m_e$. The integer values on the upper scales correspond to the oscillation numbers. Here, $1/B_0^{(a)}$ and $1/B_0^{(b)}$ are the oscillation periods for data shown in (a) and (b), respectively.

normalizing $1/B$ with the oscillation period: B_0/B. Integer values initially correspond to maxima. However, when the CR node is crossed, integer values align with minima instead. In the topmost curve for 78 GHz radiation, a second node at $\omega/\omega_c = 3/2$ is observed. When it is crossed, integer values correspond again to maxima. The data in Fig. 2(b) have been recorded at the same frequency as the bottom trace in Fig. 2(a), but for a different V_g. A comparison unveils that the MICO periodicity has changed while the node stays at the CR position.

To identify the origin of MICO, it is instrumental to systematically vary V_g, monitor changes in the oscillation period, and compare the results for different oscillation types. The outcome of such a study is summarized in Fig. 3(a). The SdH and DOS oscillations, also observed under equilibrium conditions, help to extract the density and identify when a second subband gets populated. At $V_g = 0$, where only one subband is occupied, the SdH and DOS oscillations have the same period and phase as seen in Figs. 1(c) and 1(d) (short vertical lines). Minima appear when the Fermi level is located within a cyclotron gap and an integer number n of spin degenerate Landau levels is occupied. This occurs at B fields for which $n_{s1} = 2nN_0$, with $n = 1, 2, \ldots$, $N_0 = eB/h$ is the Landau level degeneracy per spin, and n_{s1} is the density in the lowest subband. It results in a $1/B$ periodicity equal to $2e/hn_{s1}$ from which n_{s1} can be calculated. However, more generally, this expression can be used to convert any observed periodicity into a density whose meaning needs to be interpreted properly. Hereafter, the densities extracted from SdH and DOS oscillations as well as MICO will be denoted as n_l, with subscript $l = \text{SdH}$, DOS, or MICO. They have been plotted in Fig. 3(a) together with n_H deduced from the Hall resistance at low B. The latter increases with V_g at a constant rate. When tracing n_{SdH} and n_{DOS} to positive V_g in Fig. 3(a), we note that their behavior is very different. For

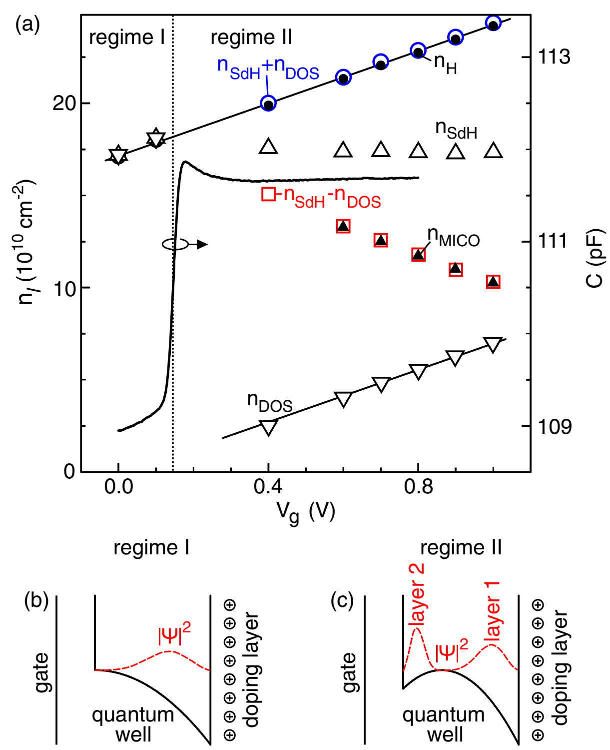

FIG. 3. (a) Gate voltage dependencies of electron densities n_l determined from 0.5 K SdH oscillations (n_{SdH}, upward open triangles), magneto-oscillations of dark capacitance (n_{DOS}, downward open triangles), MICO (n_{MICO}, upward close triangles), and Hall resistance (n_H, solid dots). The vertical dotted line separates regions I and II with one and two occupied subbands, respectively. The calculated values of $n_{\text{DOS}} + n_{\text{SdH}}$ (open circles) and $n_{\text{SdH}} - n_{\text{DOS}}$ (open squares) are shown for region II and $V_g \geq 0.4$ V. The lower thin line is drawn through the n_{DOS} data points parallel to that corresponding to the $n_H(V_g)$ dependence. The thick solid curve is the experimental dependence of capacitance versus gate voltage at $B = 0$. Potential and electron density distribution $|\Psi|^2$ in the QW are schematically shown in (b) and (c) for one and two occupied subbands, respectively.

instance, $n_{\rm SdH}$ remains approximately constant. Referring to the raw data recorded at $V_g = 1.0$ V [Fig. 1(b)], the envelope of the SdH oscillation pattern has become more complicated, but its main period indeed remains close to that at $V_g = 0$. On the other hand, $n_{\rm DOS}$ drops considerably when V_g exceeds 0.15 V. This is also apparent in the raw data of Fig. 1, where the horizontal arrows in Figs. 1(a) and 1(b) mark the oscillation periods. In Fig. 3(a) also the sum $n_{\rm SdH} + n_{\rm DOS}$ has been plotted. It coincides with n_H for $V_g > 0.15$ V. In regime I, all densities are equal: $n_{\rm SdH} = n_{\rm DOS} = n_H = n_s = n_{s1}$. We assert that all these observations can be understood straightforwardly assuming the second subband becomes occupied for $V_g > 0.15$ V.

In a wide QW with an asymmetric potential profile, subband wave functions are located at different distances from the gate, effectively mimicking a bilayer system as schematically illustrated in Fig. 3(c). For such a case, a variation of V_g primarily changes the density in the second subband or layer 2 closest to the gate and only slightly affects the charge in remote layer 1 (the first subband). Then, the DOS oscillations are determined by Landau quantization in the second subband and their periodicity is governed by the density in this subband, n_{s2}, only (for more details, see Refs. [40,41]). Back to the SdH oscillations, one may expect two sets of oscillations, determined by carrier densities in both subbands, n_{s1} and n_{s2}. In our raw data the fastest oscillations are, however, easiest to discern. They are associated with Landau quantization of the lowest subband with the largest population, n_{s1}, which remains approximately fixed since the gate electric field is screened by the electrons in the second subband. These electrons generate weaker oscillations in the envelope of the rapid oscillations from the first subband. We note that the linear $n_{s2}(V_g)$ dependence as well as nearly constant value of n_{s1} shown in Fig. 3(a) are similar to those reported in other studies of unbalanced bilayer electron systems (see, for example, Refs. [42,43] for single and double quantum wells, respectively). The Hall density n_H corresponds to the total density n_s. This interpretation of the data is strongly supported by the experimentally established relation $n_H = n_{\rm DOS} + n_{\rm SdH}$. Then, we finally conclude that $n_{\rm DOS} = n_{s2}$ and $n_{\rm SdH} = n_{s1}$. Figure 3(a) also contains the density extracted from MICO, $n_{\rm MICO}$. Apparently it is identical to $n_{\rm SdH} - n_{\rm DOS}$, which in view of the above discussion is equivalent to the subband population difference: $n_{\rm MICO} = n_{s1} - n_{s2}$.

Clearly, the response to radiation is very different in ρ_{xx} and the magnetocapacitance. It follows that MICO cannot be explained in terms of a MW-induced variation of the conductivity. The extracted density from MICO points to its origin, since the condition $n_{s1} - n_{s2} = 2nN_0$ is equivalent to $\Delta \equiv \varepsilon_2 - \varepsilon_1 = n\hbar\omega_c$, where ε_j ($j = 1, 2$) are the subband energies. At this commensurability condition, Landau levels of the two subbands are aligned. We, therefore, argue that MICO reflect a MW-induced charge redistribution among the two subbands whose magnitude oscillates with B. This is detected in the capacitance since, in our sample, it selectively responds to occupation of the second subband. This interpretation is further corroborated by the capacitance step observed in Fig. 3(a) at $V_g \approx 0.15$ V. This step is caused by occupation of the second subband (i.e., formation of the second layer) with a center of mass of the wave function located approximately 20 nm closer to the gate than that of the 2DES in regime I at $V_g \lesssim 0.15$ V [compare Figs. 3(b) and 3(c)]. It demonstrates sensitivity of our measurements to variation of the charge distribution in the QW. For the sake of completeness, we note that also magnetointersubband oscillations (MISO) with a period determined by the relation $\Delta = n\hbar\omega_c$ may occur in the magnetoresistance due to intersubband scattering [44–48]. They can be strongly affected by radiation, which may introduce nodes [25,49]. They can be explained by both the nonequilibrium distribution function and displacement mechanisms [25,50]. In Fig. 1(b), the MISO are not visible since at 0.5 K they are masked by the SdH oscillations and by the MIRO in the absence and presence of the MW radiation, respectively.

To substantiate our assertion that the magnetocapacitance oscillations prove that microwaves create a nonequilibrium distribution function oscillating with energy due to Landau quantization, we have analyzed our results within a distribution function model generalized to the case of two occupied subbands [25]. The equation for the MW-induced correction $\delta f(\varepsilon)$ to the Fermi distribution function $f_F(\varepsilon)$ in a balanced double-quantum-well structure reads as follows [25]:

$$\delta f(\varepsilon) \simeq \frac{\hbar\omega}{2}\frac{\partial f_F}{\partial \varepsilon} P_\omega \sin\frac{2\pi\omega}{\omega_c} \sum_{j=1,2} d_j \sin\frac{2\pi(\varepsilon - \varepsilon_j)}{\hbar\omega_c}. \quad (1)$$

The dimensionless factor P_ω is proportional to the MW power absorbed by the 2DES. This equation is derived to first order with respect to the small Dingle factors, $d_j = \exp(-\pi/\omega_c\tau_j)$, for each subband and under the assumptions that $\hbar\omega \ll kT \ll \varepsilon_F - \varepsilon_j$. Here, τ_j is the electron quantum lifetime in the jth subband and ε_F is the Fermi energy. Within this framework of approximations, the density of states in a subband is given by

$$D_j(\varepsilon) = \frac{m^*}{\pi\hbar^2}\left(1 - d_j \cos\frac{2\pi(\varepsilon - \varepsilon_j)}{\hbar\omega_c}\right). \quad (2)$$

The MW-induced variation of the density in the first subband ($\varepsilon_1 < \varepsilon_2$) is equal to

$$\delta n_{s1} = -\delta n_{s2} = \int_{\varepsilon_1}^{\infty} D_1(\varepsilon)\delta f(\varepsilon) d\varepsilon$$
$$= -d_1 d_2 \frac{m^*}{\pi\hbar^2}\frac{\hbar\omega}{4} P_\omega \sin\frac{2\pi\omega}{\omega_c} \sin\frac{2\pi(\varepsilon_2 - \varepsilon_1)}{\hbar\omega_c}. \quad (3)$$

When $\varepsilon_2 - \varepsilon_1 = \Delta \gg \hbar\omega$, Eq. (3) describes magneto-oscillations with a periodicity determined by the commensurability between the cyclotron energy and the subband spacing: $\Delta = n\hbar\omega_c$. The beating pattern and nodes are caused by the factor $\sin(2\pi\omega/\omega_c)$. The nodes are located at $\omega/\omega_c = (n+1)/2$. This oscillation pattern described by Eq. (3) matches all the observed features of MICO. These oscillations should also persist in an unbalanced system in which the centers of mass of the wave functions of the two subbands are spatially separated. Then the oscillating redistribution of electrons between the subbands (i.e., the layers) $\delta n_{s1} = -\delta n_{s2}$ produces oscillations in the capacitance. This accounts for our experimental observations.

In summary, by implementing a new experimental approach to study nonequilibrium phenomena in 2DES, we have discovered microwave-induced magneto-oscillations of an electrical capacitance. We have shown that these oscillations reflect redistribution of electrons between two occupied subbands which oscillates with magnetic field due to nontrivial distribution of electrons among Landau levels. Our observation establishes unequivocally the importance of this nonequilibrium distribution function scenario, which was developed to explain MIRO.

We acknowledge fruitful discussions with I. A. Dmitriev. Experiment and data evaluation of this work were supported by the Russian Scientific Foundation (Grant No. 14-12-00599). J. H. S. and V. U. acknowledge support from the GIF.

[1] M. A. Zudov, R. R. Du, J. A. Simmons, and J. L. Reno, Phys. Rev. B **64**, 201311(R) (2001).
[2] P. D. Ye, L. W. Engel, D. C. Tsui, J. A. Simmons, J. R. Wendt, G. A. Vawter, and J. L. Reno, Appl. Phys. Lett. **79**, 2193 (2001).
[3] R. G. Mani, J. H. Smet, K. von Klitzing, V. Narayanamurti, W. B. Jonson, and V. Umansky, Nature (London) **420**, 646 (2002).
[4] M. A. Zudov, R. R. Du, L. N. Pfeiffer, and K. W. West, Phys. Rev. Lett. **90**, 046807 (2003).
[5] S. I. Dorozhkin, V. Umansky, L. N. Pfeiffer, K. W. West, K. Baldwin, K. von Klitzing, and J. H. Smet, Phys. Rev. Lett. **114**, 176808 (2015).
[6] D. F. Kärcher, A. V. Shchepetilnikov, Yu. A. Nefyodov, J. Falson, I. A. Dmitriev, Y. Kozuka, D. Maryenko, A. Tsukazaki, S. I. Dorozhkin, I. V. Kukushkin, M. Kawasaki, and J. H. Smet, Phys. Rev. B **93**, 041410(R) (2016).
[7] M. A. Zudov, O. A. Mironov, Q. A. Ebner, P. D. Martin, Q. Shi, and D. R. Leadley, Phys. Rev. B **89**, 125401 (2014).
[8] R. Yamashiro, L. V. Abdurakhimov, A. O. Badrutdinov, Yu. P. Monarkha, and D. Konstantinov, Phys. Rev. Lett. **115**, 256802 (2015).
[9] I. A. Dmitriev, A. D. Mirlin, D. G. Polyakov, and M. A. Zudov, Rev. Mod. Phys. **84**, 1709 (2012).
[10] Y. M. Beltukov and M. I. Dyakonov, Phys. Rev. Lett. **116**, 176801 (2016).
[11] J. H. Smet, B. Gorshunov, C. Jiang, L. Pfeiffer, K. West, V. Umansky, M. Dressel, R. Meisels, F. Kuchar, and K. von Klitzing, Phys. Rev. Lett. **95**, 116804 (2005).
[12] T. Herrmann, I. A. Dmitriev, D. A. Kozlov, M. Schneider, B. Jentzsch, Z. D. Kvon, P. Olbrich, V. V. Bel'kov, A. Bayer, D. Schuh, D. Bougeard, T. Kuczmik, M. Oltscher, D. Weiss, and S. D. Ganichev, Phys. Rev. B **94**, 081301(R) (2016).
[13] O. V. Zhirov, A. D. Chepelianskii, and D. L. Shepelyansky, Phys. Rev. B **88**, 035410 (2013).
[14] S. A. Mikhailov, Phys. Rev. B **83**, 155303 (2011).
[15] M. A. Zudov, Phys. Rev. B **92**, 047301 (2015).
[16] S. A. Mikhailov, Phys. Rev. B **92**, 047302 (2015).
[17] R. L. Willett, L. N. Pfeiffer, and K. W. West, Phys. Rev. Lett. **93**, 026804 (2004).
[18] A. A. Bykov, JETP Lett. **87**, 233 (2008).
[19] S. I. Dorozhkin, I. V. Pechenezhskiy, L. N. Pfeiffer, K. W. West, V. Umansky, K. von Klitzing, and J. H. Smet, Phys. Rev. Lett. **102**, 036602 (2009).
[20] I. A. Dmitriev, S. I. Dorozhkin, and A. D. Mirlin, Phys. Rev. B **80**, 125418 (2009).
[21] S. I. Dorozhkin, I. A. Dmitriev, and A. D. Mirlin, Phys. Rev. B **84**, 125448 (2011).
[22] S. I. Dorozhkin, JETP Lett. **77**, 577 (2003).
[23] I. A. Dmitriev, A. D. Mirlin, and D. G. Polyakov, Phys. Rev. Lett. **91**, 226802 (2003).
[24] I. A. Dmitriev, M. G. Vavilov, I. L. Aleiner, A. D. Mirlin, and D. G. Polyakov, Phys. Rev. B **71**, 115316 (2005).
[25] S. Wiedmann, G. M. Gusev, O. E. Raichev, T. E. Lamas, A. K. Bakarov, and J. C. Portal, Phys. Rev. B **78**, 121301(R) (2008).
[26] A. O. Badrutdinov, L. V. Abdurakhimov, and D. Konstantinov, Phys. Rev. B **90**, 075305 (2014).
[27] A. D. Chepelianskii, M. Watanabe, K. Nasyedkin, K. Kono, and D. Konstantinov, Nat. Commun. **6**, 7210 (2015).
[28] T. P. Smith, B. B. Goldberg, P. J. Stiles, and M. Heiblum, Phys. Rev. B **32**, 2696 (1985).
[29] V. I. Ryzhii, Fiz. Tverd. Tela (Leningrad) **11**, 2577 (1969) [Sov. Phys. Solid State **11**, 2078 (1970)].
[30] V. I. Ryzhii, R. A. Suris, and B. S. Shchamkhalova, Fiz. Tekh. Poluprovodn. **20**, 2078 (1986) [Sov. Phys. Semicond. **20**, 1299 (1986)].
[31] A. C. Durst, S. Sachdev, N. Read, and S. M. Girvin, Phys. Rev. Lett. **91**, 086803 (2003).
[32] V. Ryzhii, A. Chaplik, and R. Suris, JETP Lett. **80**, 363 (2004).
[33] M. G. Vavilov and I. L. Aleiner, Phys. Rev. B **69**, 035303 (2004).
[34] I. A. Dmitriev, M. Khodas, A. D. Mirlin, D. G. Polyakov, and M. G. Vavilov, Phys. Rev. B **80**, 165327 (2009).
[35] C. L. Yang, M. A. Zudov, T. A. Knuuttila, R. R. Du, L. N. Pfeiffer, and K. W. West, Phys. Rev. Lett. **91**, 096803 (2003).
[36] O. M. Fedorych, M. Potemski, S. A. Studenikin, J. A. Gupta, Z. R. Wasilewski, and I. A. Dmitriev, Phys. Rev. B **81**, 201302(R) (2010).
[37] A. D. Levin, Z. S. Momtaz, G. M. Gusev, O. E. Raichev, and A. K. Bakarov, Phys. Rev. Lett. **115**, 206801 (2015).
[38] See Supplemental Material at http://link.aps.org/supplemental/10.1103/PhysRevLett.117.176801 for a sample design and details of measurements.

[39] A. T. Hatke, M. A. Zudov, J. D. Watson, M. J. Manfra, L. N. Pfeiffer, and K. W. West, Phys. Rev. B **87**, 161307(R) (2013).
[40] V. T. Dolgopolov, A. A. Shashkin, E. V. Deviatov, F. Hastreiter, M. Hartung, A. Wixforth, K. L. Campman, and A. C. Gossard, Phys. Rev. B **59**, 13235 (1999).
[41] S. I. Dorozhkin, Pis'ma Zh. Eksp. Teor. Fiz. **103**, 578 (2016) [JETP Lett. **103**, 513 (2016)].
[42] H. L. Störmer, A. C. Gossard, and W. Wiegmann, Solid State Commun. **41**, 707 (1982).
[43] X. Ying, S. R. Parihar, H. C. Manoharan, and M. Shayegan, Phys. Rev. B **52**, R11611 (1995).
[44] V. M. Polyanovskii, Fiz. Tekh. Poluprovodn. **22**, 2230 (1988) [Sov. Phys. Semicond. **22**, 1408 (1988)].
[45] P. T. Coleridge, Semicond. Sci. Technol. **5**, 961 (1990).
[46] D. R. Leadley, R. J. Nicholas, J. J. Harris, and C. T. Foxon, Semicond. Sci. Technol. **5**, 1081 (1990).
[47] D. R. Leadley, R. Fletcher, R. J. Nicholas, F. Tao, C. T. Foxon, and J. J. Harris, Phys. Rev. B **46**, 12439 (1992).
[48] M. E. Raikh and T. V. Shahbazyan, Phys. Rev. B **49**, 5531 (1994).
[49] A. A. Bykov, D. R. Islamov, A. V. Goran, and A. I. Toropov, JETP Lett. **87**, 477 (2008).
[50] S. Wiedmann, G. M. Gusev, O. E. Raichev, A. K. Bakarov, and J. C. Portal, Phys. Rev. B **81**, 085311 (2010).